www.elsevier.com/locate/memsci

Water Diffusion in Zeolite Membranes: Molecular Dynamics Studies on Effects of Water Loading and Thermostat

Kuk Nam Han, Stefano Bernardi, Lianzhou Wang, Debra J. Searles

PII: S0376-7388(15)30128-9
DOI: http://dx.doi.org/10.1016/j.memsci.2015.08.033
Reference: MEMSCI13920

To appear in: *Journal of Membrane Science*

Received date: 20 March 2015
Revised date: 13 August 2015
Accepted date: 14 August 2015

Cite this article as: Kuk Nam Han, Stefano Bernardi, Lianzhou Wang and Debra J. Searles, Water Diffusion in Zeolite Membranes: Molecular Dynamics Studies on Effects of Water Loading and Thermostat, *Journal of Membrane Science* http://dx.doi.org/10.1016/j.memsci.2015.08.033

Water Diffusion in Zeolite Membranes: Molecular Dynamics Studies on Effects of Water Loading and Thermostat

Kuk Nam Han,[a,b] *Stefano Bernardi,*[a] *Lianzhou Wang*[a,b] *and Debra J. Searles*[a,c]

[a] Centre for Theoretical and Computational Molecular Science, Australian Institute for Bioengineering and Nanotechnology, The University of Queensland, Brisbane, Qld 4072

[b] Nanomaterials Centre, School of Chemical Engineering and Australian Institute for Bioengineering and Nanotechnology, The University of Queensland, Brisbane, Qld 4072

[c] School of Chemistry and Molecular Biosciences, The University of Queensland, Brisbane, Qld 4072

* Corresponding Author: D. J. Searles

Tel: +61-7-33463939

Fax: +61-7-33463992

E-mail: d.bernhardt@uq.edu.au

** Co-corresponding author: L. Wang (l.wang@uq.edu.au)

Abstract

Molecular dynamics simulations were employed to investigate diffusion and structural properties of water molecules confined in one-dimensional zeolites. Several water loadings and thermostatting methods were used, and insight into the effects of these was obtained by comparing diffusion and structural properties. Water diffusion was characterised via mean square displacements (self and collective diffusivities) and radial distribution functions enabled the structural ordering of water for different pore sizes and loadings to be compared. Interestingly at lower loadings, molecules tend to form clusters and move collectively, while at higher loadings, the self-diffusion coefficient in the pores is similar to that in bulk water. The length of the simulation cell was varied to determine the system size effects on the results, and narrow pores were also investigated in order to examine how this affected the effectiveness of water transport through the zeolite.

Keywords: zeolite; membrane; molecular dynamics; thermostat; water diffusion.

1. Introduction

Zeolites and zeolite-like materials (e.g. metal organic frameworks) have attracted considerable attention over the last few decades due to their versatile industrial applications as materials for catalysis, absorption, and molecular sieving [1, 2]. Their flexibility stems from the large range of nanoporous crystal structures [3-5] that their chemistry allows them to form. In addition, their chemical composition and reactivity can be varied. Such materials have recently been employed as membrane materials [6-10]. We select zeolites that have pore sizes that are sufficiently small that small ions and molecules are expected to be excluded from the pores due to a molecular sieving effect, and focus on the diffusion coefficients of water in these materials.

Molecular dynamics (MD) simulations have proven to be a reliable method to characterise the kinetics, dynamics and thermodynamics of nanostructures at the molecular scale, enabling the probing of time and length scales which are previously difficult to access experimentally. The possibility of mimicking the behaviour of atomic and molecular clusters can therefore help to predict and successively fine tune better materials for specific applications. With the advancement of computing performance, MD simulations can be employed for bigger and more complex structures e.g. water transport across zeolitic systems [11-13].

Carbon nanotubes (CNTs) and porous graphene are alternative membrane materials that possess well-defined pores; the pore size can be under 1 nm, which is molecular sieving to small ions and molecules [14-16]. Both materials exhibit exceptional water flow rates through the pores due to the fact that the hydrophobicity as well as straightness of the pores provide water molecules inside with "hyperlubricity" [16-18]. However, from an experimental point of view, making such small and well-defined pores is very difficult to achieve. Techniques for formation of uniform pore size and high pore density materials are still far from being commercially viable for membranes [13]. In contrast, zeolites naturally exist as well-defined crystalline structures and the pores are well packed,

giving a high pore density. Due to this practical advantage, zeolites that have well-defined one-dimensional (1-D) pores of sub-nanometre diameter are proposed to have high potential as membrane materials. This work thus studies on 1-D zeolite based membranes.

Both experimental and simulation results have identified that water in hydrophobic and/or nanoporous structures forms clusters at some loadings [19-21]. Small-angle x-ray scattering (SAXS) experiments and grand canonical Monte Carlo (GCMC) studies have shown that water molecules begin to form clusters that are 6 Å in diameter at 0.6 relative pressure (P/P_0) within a 11 Å width slit-pore and the cluster size becomes bigger with increasing the pressure (higher water loading) due to combination of clusters [19]. Also, it has been found that water assemblies of 15 Å diameter are formed and the structure has ice-like order in slit-pores of 16.3 Å in width at P/P_0 = 0.6 using x-ray diffraction (XRD) measurements and reverse Monte Carlo simulations [21]. Recently, some interesting studies have been carried out for slit-pores of different widths (7 and 11 Å) and at different pressures (P/P_0), revealing that the kinetics of water assembly is dominantly influenced by the pore width at low pressure (under P/P_0 = 0.5) and water adsorption rate is faster for the narrower pores at just above the critical pressure (0.4 for 7 Å width and 0.6 for 11 Å) [22]. In addition, cage-like pores (LTA-type zeolite) can also hold water clusters: α-cages with 10 Å diameter have 24 molecules in a cluster, whereas β-cages with 6 Å have 4 molecules [20]. Despite these efforts, understanding water behaviour in nanopores is still far from complete.

As we expect water clustering to have a significant impact on water diffusivity and in particular on the transport diffusion coefficient, in this work we will examine structural and dynamical properties of zeolite-confined water in relation to cluster size and stability. In previous work [12, 23-25], water diffusivity in zeolites has been studied by considering self-diffusion coefficients, which quantify the rate of diffusion of a single molecule within a fluid in equilibrium, and the simulation results have been validated by comparison with experiment. In the present work, collective diffusion coefficients, which quantify the flow of molecules, were also calculated since the fluid flux is related to the

collective diffusivity and is therefore important for assessing the suitability of zeolites as a membrane. At very low densities, the self and collective diffusion coefficients become equal, but with the higher water loadings we are considering, this is not the case.

In order that MD simulations resemble experimental conditions, temperature control algorithms, so-called thermostats, are often used. Thermostats can be classified into two major categories: stochastic thermostats, which include Andersen and Langevin (LGV) thermostats; and deterministic thermostats, which include Gaussian, Berendsen, kinetic rescaling, and Nosé-Hoover (NH) thermostats. Of the deterministic thermostats, the Nosé-Hoover and Gaussian thermostats have been shown to generate the canonical (NVT) and isokinetic canonical ensemble (NVT-iso) respectively [26], and are therefore widely used. In this work we will use a Nosé-Hoover thermostat, which gives good agreement with experimental results for molecular diffusion [27, 28], and compare the results obtained with those obtained using adiabatic (unthermostatted) simulations. Thermostats can be applied to the whole system or parts of it: in the case of zeolites they could be applied to the water, the zeolite or both. It has been found that unphysical behaviour can take place due to the misuse of thermostats, especially for heterogeneous systems such as water-absorbed in nanostructures and in nonequilibrium conditions, e.g. in the presence of flow. Often the streaming velocity rather than the peculiar velocity is thermostatted, and this can result in the thermostat doing work on the system [29].

A number of studies have compared the effects of thermostats on water diffusion when confined in porous materials. Krishnan *et al*. [30] reported their influence on pressure-driven water within carbon nanotubes. They compared NH, Berendsen and LGV thermostats, and found that the particular type of thermostat used can influence the behaviour of water confined in the smaller pores at lower temperatures [30]. We have recently found that thermostatting the framework / walls of a confined fluid rather than the whole system or just the fluid inside it (e.g. keeping the walls rigid), has a significant effect on properties of fluids undergoing Couette flow [31]. Yong and Zhang [32]

extended this work, comparing the effects of LGV, dissipative particle dynamics (DPD) and simulations with NH chain thermostats on Couette flow of Lennard-Jones particles, thermostatting walls and/or fluid and found that thermostatting the walls gave better agreement with experiments. A recent work on the diffusion rates of water through carbon nanotubes subject to pressure gradients showed discrepancies in the results obtained using different thermostatting methods [33]. All these studies show that when thermostatting is not carried out appropriately, for confined systems under flow, this can result in unphysical, and rather unpredictable, behaviour [34].

Differently to those studies, we will focus on determining diffusion coefficients using equilibrium simulations. Even in the absence of external fields or gradients, it has been observed that water can form clusters at low loadings that will flow in one direction for periods of time [35]. These clusters will therefore have a streaming component to their velocity that will change with time. It is therefore important to be sure that the thermostatting mechanism is not enhancing or diminishing this effect. For equilibrium simulations the results for uniformly thermostatted systems and unthermostatted systems should converge in the thermodynamic limit. This will be checked for the systems considered in this paper. As we are ultimately interested in studying flow under pressure gradients where thermostats are necessary to prevent the system from heating up [27] it is important to check that at equilibrium the use of wall thermostats are effective for these systems.

The purpose of this study is to gain deeper insight into changes in confined fluid flow with different loadings. We will observe if clustering of the water occurs, and what affect that has on the diffusion of water. To ensure that the behaviour we are observing is not due to the thermostatting mechanism, we examine a number of different thermostats. These results will be of use in future studies of zeolitic systems as membrane candidates.

2. Background and Methods

2.1. Water Structure and Transport Properties

In this work, we consider the structure and transport of water in zeolite nanopores, and consider how these vary with loading and thermostatting mechanisms. As noted above, clustering of water in hydrophobic nanopores at moderate loading has been experimentally observed in [19, 21] by in situ SAXS and in situ XRD. In simulations, this effect can be qualitatively observed through direct visualisation of the water molecules within the pore, and can be quantitatively characterised by calculation of the radial distribution function $g(r)$ that for two particles of the same species is,

$$g(r) = \frac{N_s(r)}{V_s(r)} \times \frac{1}{\rho} \tag{1}$$

where N_s is the number of particles in a spherical shell of radius between r and $r + dr$ and volume V_s, centred on a particle of interest, and ρ is the average particle number density for the whole system. This is most appropriate for study of spherically symmetric systems where it becomes equal to 1 when the particles are uniformly distributed. It can be measured experimentally by scattering spectroscopy. For the asymmetric systems considered here where the water molecules are confined to a pore, it is more useful to consider a function which is modified to account for the confinement $g(r)_{pore}$,

$$g(r)_{pore} = g(r) \times \frac{V_s(r)}{V_{ps}(r)} \times \frac{\rho}{\rho_p} \approx g(r) \times \frac{V_s(r)}{2\pi {r_p}^2 dr} \times \frac{\rho}{\rho_p} \tag{2}$$

where V_{ps} represents the accessible volume of the pore shell between r and $r + dr$ (i.e. the portion of the spherical shell that is in the pore), ρ_p is defined as the particle number density of the pore and r_p

is the radius of the pore. Here we use the approximation that $V_{ps} \approx 2\pi r_p^2 dr$ which will be accurate at large r and overestimate $g(r)_{pore}$ at $r \approx r_p$, however since the accessible pore volume can only be estimated, this approximation is accepted. Use of $g(r)_{pore}$ is appropriate for the characterisation of density profiles in one dimensional pores and will have a value of 1 at all r if the particles are uniformly distributed in the pore.

Transport within a pore can be quantified through the self-diffusion coefficient D_s, and the collective diffusion coefficient D_c which is directly related to the transport diffusion coefficient [36]. Self-diffusion represents the spontaneous mixing of particles among themselves, as such it is an indicator of molecular mobility. Experimentally, self-diffusivity can be determined by using pulsed field gradient nuclear magnetic resonance (PFG-NMR) [23] and quasielastic neutron scattering (QENS) measurements [36, 37], however from the self-diffusivity measurement, discrimination of collective motion, i.e. transport of nano-sized water droplet, is not possible. The collective diffusivity, which is more important parameter for evaluation of a zeolite as a potential membrane. The transport diffusivity is given by the ratio of the flux of molecules in the fluid due to a concentration gradient [38], ($J = -D_t \, \partial C/\partial z$ where J is the flux, D_t is the transport diffusion coefficient, C is the concentration, and z is the position), and is directly related to the collective diffusion coefficient through a thermodynamic factor [36] ($D_t = 1/(k_B T)\,(\partial \mu/\partial \ln C)_T D_c$ where μ is the chemical potential). Thus, the membrane performance in terms of flux can be evaluated by the collective diffusion coefficient. Transport/collective diffusivities in zeolites have been experimentally measured by QENS (e.g. [37]) and by direct experimental measurements (e.g. [39]).

The self-diffusion coefficient can be obtained by monitoring the mean square displacement (MSD) of each water molecule within the system, and if the motion is diffusive it will be given by the Einstein relationship,

$$MSD(t) = \frac{1}{N}\lim_{t\to\infty}\langle\sum_{i=1}^{N}|\boldsymbol{r}_i(t) - \boldsymbol{r}_i(0)|^2\rangle = 2dD_s t \quad (3)$$

where $r_i(t)$ is the position of the ith particle at time t, d is the system dimensionality and N is the number of molecules in the pore. The collective diffusion coefficient monitors the MSD of the centre-of-mass (com) of all the water molecules in a pore

$$MSD_{cm}(t) = \frac{1}{M}\lim_{t\to\infty}\langle\sum_{j=1}^{M}\left|\boldsymbol{r}_{cm,j}(t) - \boldsymbol{r}_{cm,j}(0)\right|^2\rangle = 2dD_c t \quad (4)$$

where M is the number of pores and $\boldsymbol{r}_{cm,j} = 1/N\sum_{i=1}^{N} r_i$ is the centre-of-mass of the N water molecules in the jth pore. In the limit of low density, or if the water moves as a cluster, D_s and D_c will converge to the same value.

In the bulk (i.e. isotropic systems), each direction contributes equally to the diffusion coefficients:

$$D_x = D_y = D_z = D \quad (5)$$

where

$$2D_\alpha t = \frac{1}{N}\lim_{t\to\infty}\langle\sum_{i=1}^{N}\left|r_{\alpha,i}(t) - r_{\alpha,i}(0)\right|^2\rangle, \quad \alpha = x, y, z \quad (6)$$

D_x, D_y, D_z represent diffusion coefficients in x, y, z direction, respectively, and D is a global diffusion coefficient.

In one-dimensional pores however, the water diffusion is constricted to a pore along the z-axis and the relationship between D and D_z changes

$$\frac{1}{3}D_z \cong D \quad (7)$$

2.2. Simulations Algorithms

For our simulations we used an all-atom model and periodic boundary conditions (PBCs) in all directions. We consider a number of different molecular dynamics algorithms/ensembles: (i) constant volume and energy (NVE); (ii) constant volume with the temperature of the full system thermostatted (NVT); (iii) constant pressure with the temperature of the full system thermostatted (NPT); (iv) constant pressure and enthalpy (NPH); (v) constant volume with the temperature of the water thermostatted (NVT-w); (vi) constant volume with the temperature of the zeolite thermostatted (NVT-z). The simplest simulation approach is to carry out NVE simulations where the dynamics is simply Newtonian and the system samples a microcanonical distribution [40]. All calculations were carried out using LAMMPS [41-43].

Thermostatted dynamics is often used to generate a canonical distribution (NVT) and closely mimic experimental conditions. In this work this is achieved using a Nosé-Hoover chain thermostat [44], which links the system to multiple fictitious heat baths with the heat flowing in and out of the system in order to keep the average temperature at the target value. A damping parameter Q, determines the strength of the bath coupling. The value of Q will not change the ensemble, but it will affect the instantaneous rate of change of energies.

The pressure can also be controlled using a Nosé-Hoover barostat with a damping parameter, W_g, generating a NPH ensemble or an NPT ensemble when combined with a thermostat. As well as thermostatting the whole system, either the water or zeolite can be thermostatted. Thermostatting the zeolite only is particularly useful when simulating flow i.e. when it is important that the streaming velocity of the water is not misinterpreted as a contribution to the thermal energy.

The equations of motion for our system are,

$$\dot{\mathbf{q}}_i = \frac{\mathbf{p}_i}{m_i} + \frac{\mathbf{p}_g}{W_g}\mathbf{q}_i$$

$$\dot{\mathbf{p}}_\mathrm{i} = \mathbf{F}_\mathrm{i} - \frac{\mathbf{p}_\mathrm{g}}{\mathrm{W_g}}\mathbf{p}_\mathrm{i} - \frac{1}{N_f}\frac{\mathrm{Tr}[\mathbf{p}_g]}{W_g}\mathbf{p}_\mathrm{i} - \frac{p_\xi}{\mathrm{Q}}\mathbf{p}_\mathrm{i}$$

$$\dot{\xi}_k = \frac{p_{\xi k}}{Q_k} \quad \text{for } k\text{=}1,\ldots,\mathrm{M}$$

$$\dot{p}_{\xi 1} = \sum_{\mathrm{i}=1}^{\mathrm{N}} \frac{\mathbf{p}_\mathrm{i}^2}{m_i} + \frac{1}{W_g}\mathrm{Tr}[\mathbf{p}_g^t \mathbf{p}_g] - (N_f + d^2)kT_0 - p_{\xi 1}\frac{p_{\xi 2}}{Q_2}$$

$$\dot{p}_{\xi k} = \left(\frac{p_{\xi k-1}^2}{Q_{k-1}} - kT_0\right) - p_{\xi k}\frac{p_{\xi k+1}}{Q_{k+1}} \quad \text{for } k\text{=}2,\ldots,M-1$$

$$\dot{p}_{\xi M} = \left(\frac{p_{\xi M-1}^2}{Q_{M-1}} - kT_0\right) \tag{8}$$

where $\mathbf{q}_i$ represents the position of a given particle i having mass of m_i, $\mathbf{p}_i$ is the momentum of particle i and $\mathbf{F}_i$ denotes force exerted on the particle i. The term $\mathbf{p}_g$ is the modularly invariant form of the cell momenta [42, 43], ξ_k and $p_{\xi k}$ are the thermostat variable and its conjugated momentum of the kth thermostat, respectively. W_g and Q_k are the mass constants of barostat and kth thermostat respectively, and control the oscillation frequency of the instantaneous pressure and temperature. N_f is the number of degrees of freedom and T_0 is the target temperature. There are several possible implementations of the Nosé-Hoover NPT equations, and this follows that used in LAMMPS [41-43].

By considering the different molecular dynamics algorithms considered above, we will be able to check that the thermostatting mechanism does not influence the structure and dynamics of the water molecules in the zeolite pores.

2.3. Zeolite membrane construction and potential

Several MD simulations were carried out at different water loadings. We mostly focused on the VET framework as a membrane model which possesses cylindrical-like one dimensional channels with hydrophobic internal walls composed of Si and O only. All pores in the framework that are accessible to the water are approximately cylindrical and the accessible volume for water molecules is 78.2 $Å^3$/1000 $Å^3$. According to crystallographic data [3, 45], the effective diameter of the pore is 5.9 Å, and this is anticipated to be a useful material for applications such as water purification since pores of this size are expected to let water pass through while fully rejecting small ions and molecules including hydrated sodium and chloride ions. A unit cell of VET was taken from the crystallographic database [3], the unit cell size is 13.048 x 13.048 x 4.948 Å for x, y, z coordinates, respectively and the angles between all lattice vectors are 90°, it consists of 17 Si and 34 O atoms with a single 5.9 Å pore. In all the calculations we use a periodic simulation box with the pore aligned with the z-axis. The simulation box was composed of 2 x 2 crystallographic unit cells in the x, y-coordinates, and from 7 unit cells in the z-direction, making an initial cell size of 26.096 x 26.096 x 34.636 Å with 476 Si and 952 O (see Fig. 1(a), (b)). In order to check the stability of the zeolite structure using the selected force field and to relax the structure at the desired temperature and pressure, an equilibration simulation run was carried out on the framework with constant pressure and temperature ensemble (NPT) at 300 K and 1 atm before placing water molecules inside. In order to examine the effects of pore width on the results, the TON zeolite was also considered. This material has the same chemical composition but a smaller pore width (4.6 x 5.7 Å). Like VET, TON has 1-D channels, however the pores are slightly elliptic and the unit cell size is 13.859 x 17.420 x 5.038 Å for x, y, z coordinates, respectively, with the angles between all lattice vectors being 90°. The unit cell comprising 24 Si and 48 O atoms, was replicated to construct a 2 x 2 x 7 simulation box, with the z-axis aligned with the pore. The simulation size is 27.718 x 34.840 x 35.266 Å with 672 Si and 1344 O (see Fig. 1(c), (d)). The accessible volume of the TON membrane is 80.4 $Å^3$/1000 $Å^3$. The TIP4P-Ew water model [46] was used, as it gives reasonable agreement

with experimental data in terms of structure and diffusion rates [15, 46, 47]. This model consists of three atoms (H, O, H) rigidly constrained and one massless flexible charged particle attached to the oxygen. A Lennard-Jones (LJ) intermolecular interaction exists between the oxygen atoms:

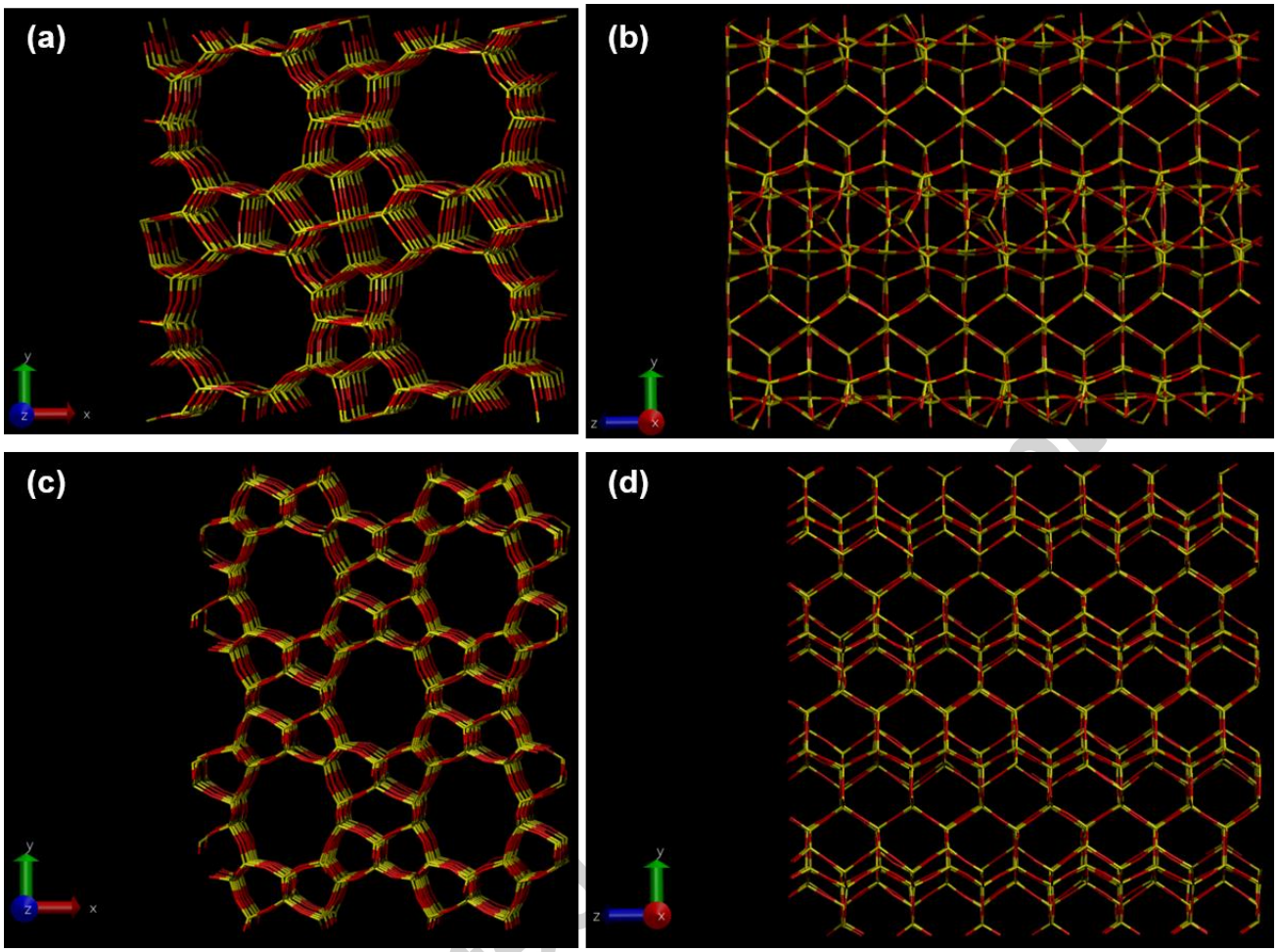

Fig. 1. Simulation cells used for the two zeolites considered (zeolites represented by wires, oxygen coloured in red and silicon in yellow): VET views along the (a) z-axis (slightly distorted towards x-direction to better show the geometry of pores, the representations viewed in this direction were applied in the same manner in the rest of the paper) and (b) x-axis; and TON views along the (c) z-axis; and (d) x-axis.

$$U(r_{ij}) = 4\varepsilon\left[\left(\frac{\sigma}{r_{ij}}\right)^{12} - \left(\frac{\sigma}{r_{ij}}\right)^{6}\right] \quad (9)$$

where ε is the well depth of potential, r_{ij} is the distance between atoms, and σ is the distance at which the LJ energy is zero [48]. In addition there is a Coulombic potential between charges on the hydrogen atoms and the massless particle. For interactions between the zeolite atoms and between zeolite-water interactions we used the Buckingham potential

$$U(r_{ij}) = A\, exp\left(-\frac{r_{ij}}{\rho}\right) - \frac{C}{r_{ij}^6} \tag{10}$$

where A, ρ, and C are constants [49].

The three-body non-bonding interaction for the O-Si-O is given by

$$U(\theta_{jik}) = \frac{1}{2}k(\theta_{jik} - \theta_0)^2 \tag{11}$$

where k is the force constant, θ_{jik} is the angle made by the three atoms, and θ_0 is the equilibrium angle.

Parameters for zeolite-zeolite interactions were derived by Hughes *et al*. [12] who further developed the potential of Sanders *et al*. [50]. For water-zeolite interactions, we used parameters from Leeuw and Parker [51] for the interaction of α-quartz with water slightly adjusted by Hughes *et al*. in order to better match the binding energy obtained by quantum mechanical MP2 calculation.

2.4. MD simulations

The energy of the system (zeolite + water) was firstly minimised using the conjugate gradient algorithm, then equilibrated for 1 ns. A 2 ns simulation using a timestep of 1 fs in isobaric-

isothermal (NPT) ensemble followed to produce an equilibrated phase point. A NH barostat and thermostat with relaxation time of 1 ps were applied and variation in volume was monitored depending on the water loading, then the average volume for each case was employed for the constant volume simulations: NVE, NVT, NVT-z, NVT-w.

To model the long range Coulombic interactions, the particle-particle-particle mesh (PPPM) Ewald sum [52] was used. The SHAKE algorithm [53] was used to constrain the geometry of the water molecule.

Ten independent runs were performed for each system considered. All the systems were re-minimised and equilibrated for 1 ns using a timestep of 1 fs under NVT ensemble at 300 K before 2 ns production runs with different ensemble approaches were carried out: NVE, NVT, NVT-w, NVT-z, NPH, NPT.

Two different water loadings were considered: 6 and 32 water molecules per channel (7 unit cells long) for the VET zeolite for each of the thermostatting methods. Three longer channels were also considered for the smaller loading (i.e. 14, 21 and 28 unit cells with 12, 18 and 24 water molecules respectively). In addition the results for the TON zeolite with a loading of 6 water molecules per channel (7 unit cells long) were also considered. Due to the different unit cell sizes 6 water molecules in pores which are 7 unit cells correspond to different densities; using the available volumes given in [3], they would correspond to densities of 0.39 g/cm^3 for VET and 0.52 g/cm^3 for TON.

3. Results and discussion

3.1. Transport properties

We firstly considered water diffusion in the VET zeolite with simulation cells constructed with 7 unit cells in the z direction and two different water loadings, 6 and 32 water molecules/pore, which we refer to as VET6 and VET32 systems, respectively. Mean square displacement (MSD) measurements were performed to determine self and collective transport coefficients given by equations (3) and (4), respectively, as well as their components in each direction. Theoretically, diffusion under confinement is divided mainly into three types of behaviour [36]: one follows Fick's law in which MSD of the fluid increases linearly with time, the second is a slower mode referred as the anomalous diffusion [63] not strictly following the Fickian behaviour, and the other is the single-file diffusion [54-56] where the MSD is linearly proportional to the square root of time. The Fickian mechanism takes place when there are large enough pores for the guest molecules to pass each other, and when guest-guest and host-guest collisions allow movement in three-dimensions. Anomalous diffusion can occur due to confinement when fluid motion is restricted due to the channel shape. Single-file diffusion arises from the motion in pores that are small enough that the molecules cannot pass one another but the motion in one dimension unrestricted. This will occur in narrow, one-dimensional, smooth pores and can result in unusually high fluxes in narrow pores.

In this study, the water molecules diffusing through the zeolite channels are found to follow Fickian-like behaviour regardless of the ensemble and of the thermostatting mechanism employed. Linear relations for the MSD with time are obtained even though the pores are one-dimensional. This indicates that the pores are sufficiently wide that molecules can pass each other. It is also indicates that the pores are quite cylindrical with adsorption to all sites on the pore walls are of similar strength. The VET zeolite therefore resembles wide CNTs. As shown in Fig. 2, water transport in z direction is the main component of the three-dimensional diffusion and displacement in x- and y-

directions makes nearly no contribution to the MSD. In directions normal to the pore wall, the MSD increases linearly with time for a very short period (< 1 ps), until the complete restriction of motion in those directions occurs. Thus, the pores aligned one-dimensionally have both molecular and collective diffusion in one direction. The self and collective coefficients (D_{sz}, D_{cz}) with different water loadings are summarised in Table 1.

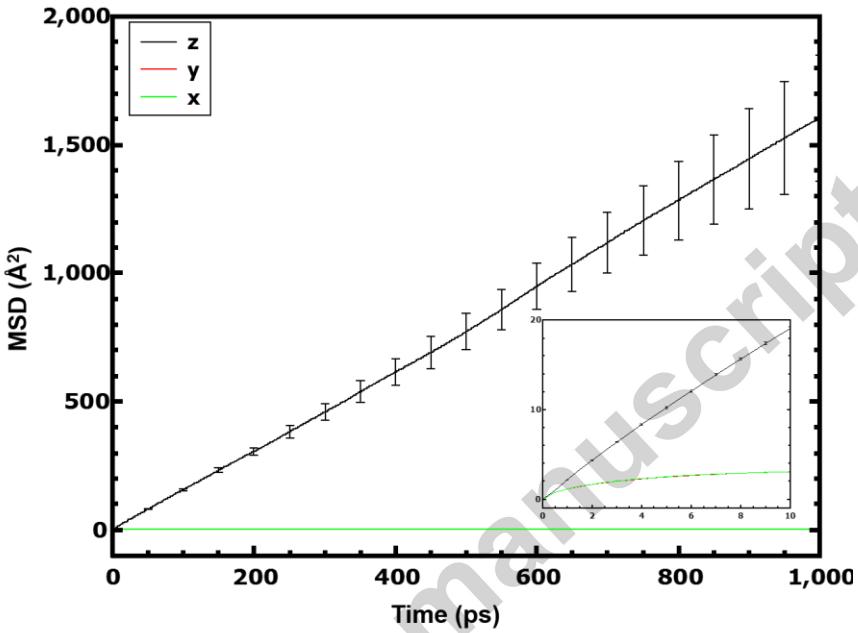

Fig. 2. MSD of the water molecules in a VET zeolite. MSD for x, y, z directions (D_{sx}, D_{sy}, D_{sz}, respectively). The inset plot is a magnified MSD at 0 to 10 ps of this figure. The periodic simulation cell had 7 unit cells in the direction parallel to the pore, and 6 water molecules in each pore. The simulation was carried out in the NVT ensemble.

As shown in Table 1 and Figures 3 and 4, MSD data is insensitive to the way in which the system is thermostatted. When small numbers of particles are considered, it would be expected that there is some difference in the results obtained with different ensembles due to finite-size effects, however despite this, even unusual ensembles (NVT-w, NPH) give very similar results to other ensembles for water diffusing through the channel.

Table 1

The z-component of the diffusion coefficients for water in zeolites

	VET6		VET32	
Ensemble	D_{sz} / 10^{-9} m^2 s^{-1}	D_{cz} / 10^{-9} m^2 s^{-1}	D_{sz} / 10^{-9} m^2 s^{-1}	D_{cz} / 10^{-9} m^2 s^{-1}
NVE	7.8 ± 1.2	6.9 ± 1.2	2.3 ± 0.1	0.5 ± 0.1
NVT	8.1 ± 1.2	7.2 ± 1.2	2.1 ± 0.1	0.5 ± 0.1
NVT-w	7.8 ± 0.9	7.2 ± 0.9	2.1 ± 0.1	0.5 ± 0.1
NVT-z	8.7 ± 1.2	8.1 ± 1.2	2.2 ± 0.1	0.5 ± 0.1
NPH	8.7 ± 1.2	8.1 ± 1.2	2.2 ± 0.1	0.5 ± 0.1
NPT	7.5 ± 0.6	6.6 ± 0.9	2.2 ± 0.1	0.4 ± 0.1

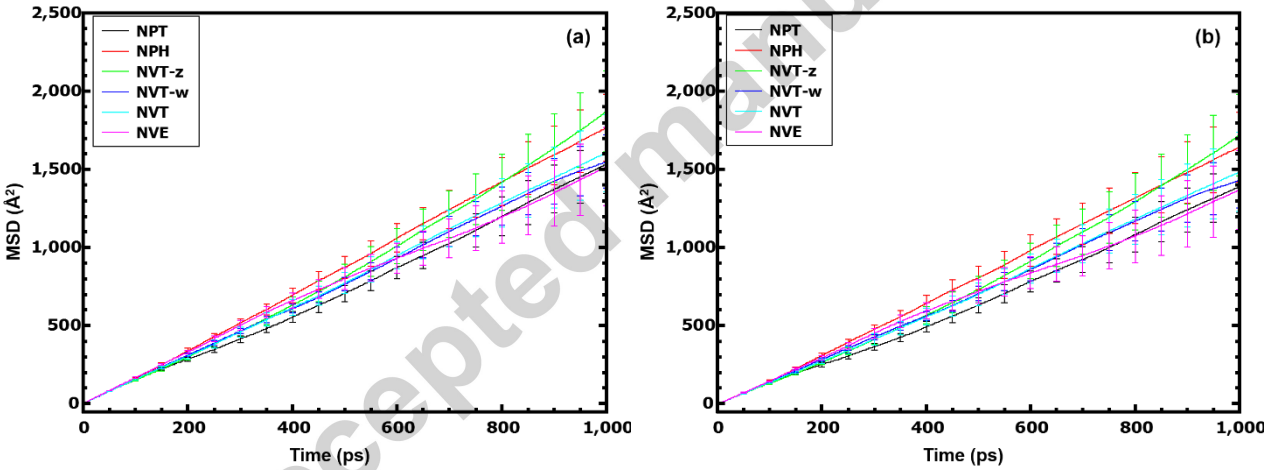

Fig. 3. MSD of the (a) molecules of water and (b) centre-of-mass of the water in a VET zeolite. The periodic simulation cell had 7 unit cells in the direction parallel to the pore, and 6 water molecules in each pore. The simulations were carried out using various thermostatting mechanisms as indicated in the legend. The terms NVT-z and NVT-w refer to cases where only the zeolite or water was thermostatted, respectively.

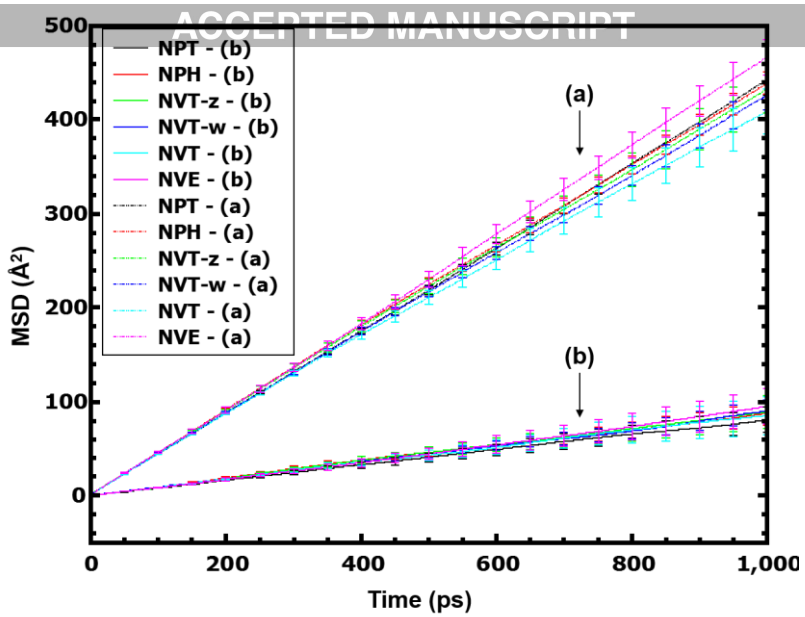

Fig. 4. MSD of the (a) molecules of water and (b) centre-of-mass of the water in a VET zeolite. The periodic simulation cell had 7 unit cells in the direction parallel to the pore, and 32 water molecules in each pore. The simulation was carried out using various thermostatting mechanisms as indicated in the legend. The terms NVT-z and NVT-w refer to cases where only the zeolite or water was thermostatted, respectively.

For a loading of 6 water molecules/pore (VET6), very similar results were obtained for the molecular and com MSD, which is consistent with the observation that water molecules inside the pores tend to form clusters and move collectively most of the time. In contrast, there is a substantial difference between the molecular MSD and the com MSD for the 32 water molecules/pore loading (VET32) where clusters do not appear to form.

The z-component of the self-diffusion coefficients for VET6 is 7.5 – 8.7 × 10^{-9} m^2 s^{-1}, while for VET32 it is 2.1 to 2.3 × 10^{-9} m^2 s^{-1}. The value of the z-component of the collective diffusion coefficient in VET32 is similar to that of bulk water (2.2 – 2.4 × 10^{-9} m^2 s^{-1}) [46, 57, 58], indicating that diffusion in this direction is similar to that in the bulk. These correspond to values of global D_s of 2.5 – 2.9 × 10^{-9} m^2 s^{-1} and 0.7 – 0.8 × 10^{-9} m^2 s^{-1} for VET6 and VET32, respectively. These values are consistent with those in Ref [12] using the same force field [12, 50], assuming 5 unit cells

formed pore used for that work (Fig. 9 of [12]). As we demonstrate below, at low loadings the values obtained for the diffusion coefficients is very sensitive to the number of unit cells used and not just to the loading.

As stated before, the collective diffusion coefficients we obtained ($6.6 – 8.1 \times 10^{-9}$ m^2 s^{-1}) are almost identical to our self-diffusion counterparts at the lower loadings, indicating that water is forming stable clusters. While at higher loadings the collective diffusivities are ca. 0.5×10^{-9} m^2 s^{-1} which is 4 times lower than their counterparts.

3.2. Structural properties

The radial distribution function (RDF) quantifies how particles are distributed around each other in a certain specified region. We used $g_{pore}(r)$ to characterise cluster sizes and distributions along the channels, where the oxygen atoms of the water molecules were selected as the species of interest.

Figure 5 shows $g_{pore}(r)$ for VET6 (5(a)) and VET32 (5(b)) and using a range of ensembles. The results obtained using the different ensembles are almost indistinguishable for both VET6 and VET32, indicating that the thermostatting/barostatting mechanisms had little effect on the structures. As it can be seen in Fig. 5(a), for VET6 there is a very high peak at short distances (ca. just below 3 Å) corresponding to the nearest neighbour water molecules, followed by another peak at about 4 Å which drops to about one at about 6 Å and then falls to a value closer to zero. The positions of the peaks correspond well with those in $g(r)$ for the oxygen atoms of TIP4P water [12, 46]. It should be noted that pore radius is about 3 Å and that the minimum distance between water molecules at the edge of one pore and those at the edge of an adjacent pore is about 7 Å. Therefore the peak at 6 Å suggests that the water molecules tend to form stable clusters, and the lengths of these clusters are about 6 Å. This phenomenon, to some extent, is consistent with the finding from the study mentioned earlier in which water molecules have a 6 Å size assembly as a starting clustering length in the 11 Å width slit-pore, water clusters with this size seem very stable [19]. Integration of $g_{pore}(r)$

to 6 Å gives a value of 6.5 (it can be higher than 6 due to the approximation for the pore shell volume made in equation (2)), indicating that all the 6 water molecules tend to be clustered together most of the time. This is verified in Fig. 6, which shows snapshots of the VET6 for the NVT simulation. Furthermore the clusters appear to be of similar length to their width, consistent with a cluster of length 6 Å. The fact that there is a small deviation in $g_{pore}(r)$ from zero at 7 Å is likely to be due to water molecules that have dissociated from the cluster for short periods of time, and at distances beyond this there may also be a contribution from water molecules in adjacent pores.

Considering Fig. 5(b), it is seen $g_{pore}(r)$ for the water oxygen atoms in VET32 is similar to $g(r)$ for bulk water [12, 46], with a value close to 1 for $r > 6$ Å. Again, this is consistent with the absence of discrete clusters of water molecules in the system at this density. This is also seen in Fig. 7 which shows snapshots of the VET32 system at various times.

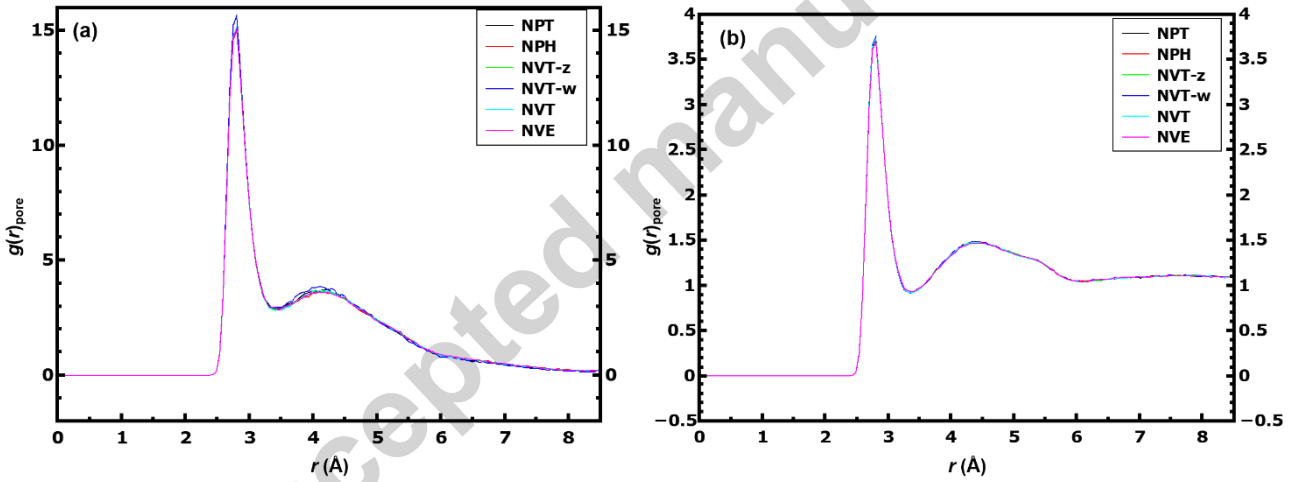

Fig. 5. The pore radial distribution function, $g_{pore}(r)$ for the O-O atoms of the water molecules in (a) VET6 and (b) VET32. The simulations were carried out using various thermostatting mechanisms as indicated in the legend. The terms NVT-z and NVT-w refer to cases where only the zeolite or water was thermostatted, respectively.

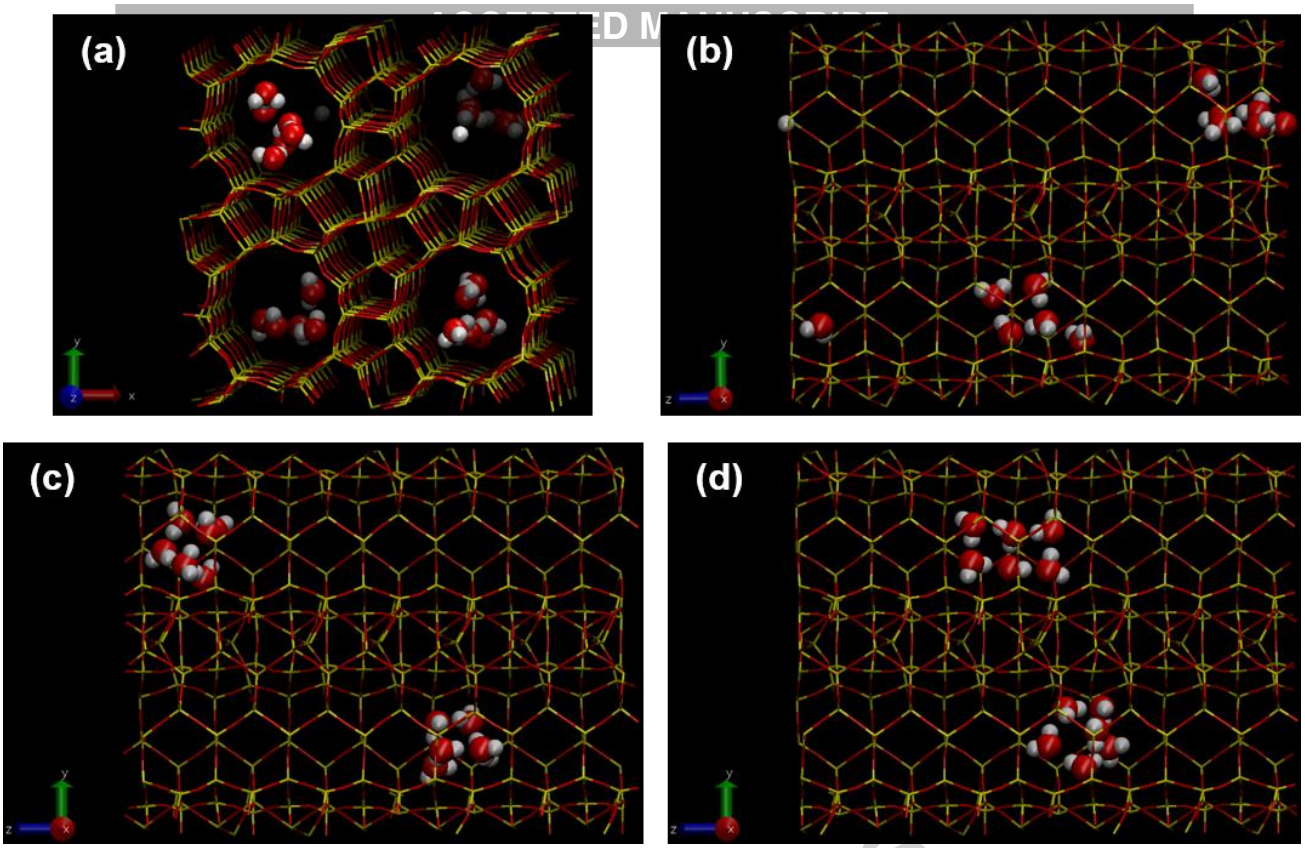

Fig. 6. Snapshots taken from the VET6 simulations (water represented by ball-and-sticks and zeolites by wires, oxygen coloured in red, hydrogen in white, silicon in yellow): (a) view along the z-axis and (b)-(d) views along the x-axis initially, at 1000 ps, and at 2000 ps, respectively. Only water molecules in the front pores are shown in (b)-(d), for better visualisation.

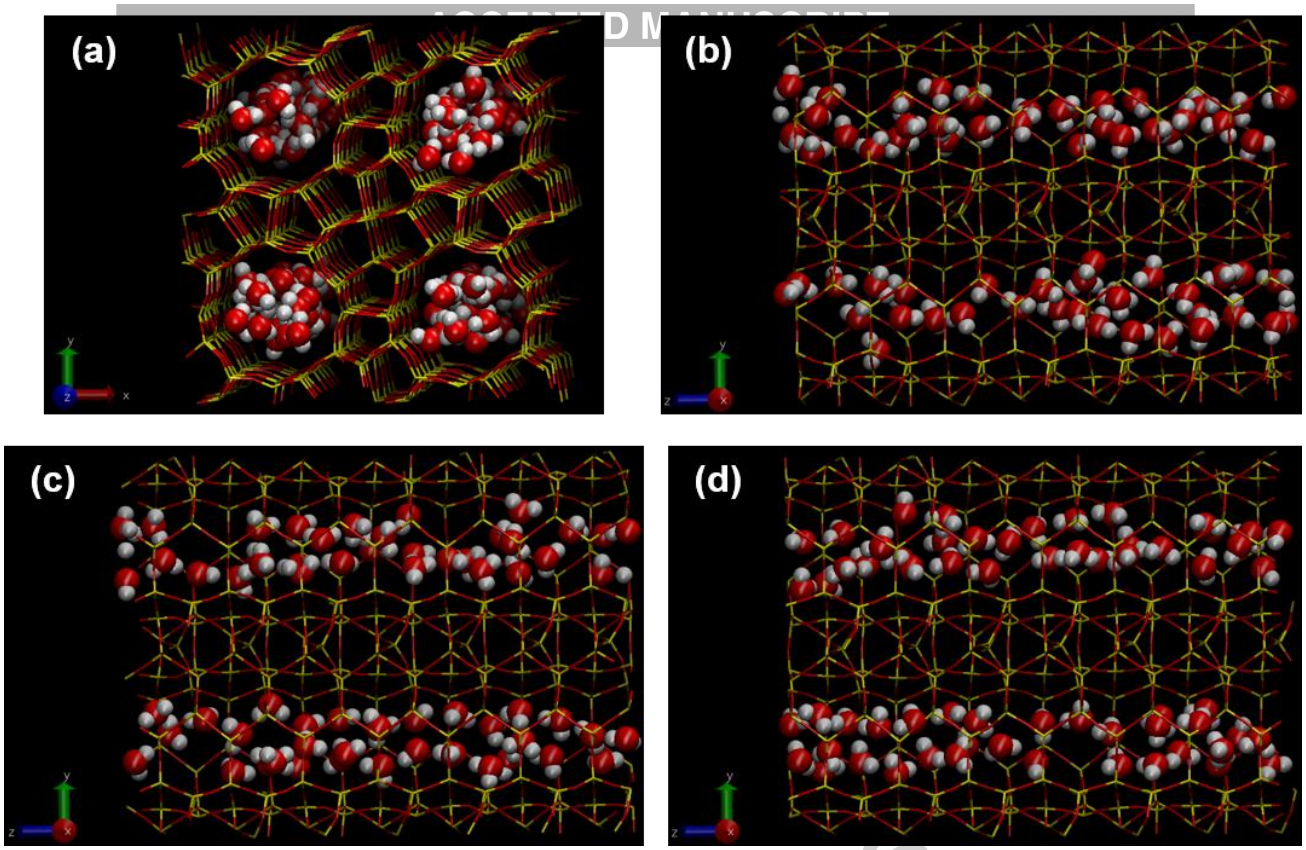

Fig. 7. Snapshots taken from the VET32 simulations (water represented by ball-and-sticks and zeolites by wires, oxygen coloured in red, hydrogen in white, silicon in yellow): (a) view along the z-axis and (b)-(d) views along the x-axis initially, at 1000 ps, and at 2000 ps, respectively. Only water molecules in the front pores are shown in (b)-(d), for better visualisation.

3.3. Effects of pore size and length on properties

In Table 2, we report the diffusion coefficients depending on the length of the simulation cell and the size of the pores. The water density for VET6, VET12-double, VET18-tri, and VET24-quad has been kept constant (0.39 g/cm^3) while the length of the simulation cell is increased i.e. double, three-times, and four-times respectively. As shown in Fig. 8, VET12-double consisted of 2 x 2 x 14 unit cells while 2 x 2 x 21 and 2 x 2 x 28 cells were used for VET18-tri and VET24-quad respectively. Because the system is periodic, we are simulating an infinitely long pore. However, the periodicity of the cell means that that the properties observed might be different from those obtained without

periodicity. In order to obtain results that are comparable with experiment, it is necessary to examine how the properties vary as the length of the periodic cell changes. In the VET6 system it was found that clusters of water molecules were formed and this places limitations on the maximum number of water molecules that can be in the cluster (i.e. 6) and the spacing between clusters. It was therefore of importance to consider the effects of increasing the length of the pore while keeping the average density constant.

Table 2

The z-component of the diffusion coefficients for water in zeolites with various loadings, different simulation cell lengths in different types of zeolites

	Water density / g cm^{-3}	Self (D_{sz}) / 10^{-9} m^2 s^{-1}	Collective (D_{cz}) / 10^{-9} m^2 s^{-1}
VET6 [a]	0.39	8.1 ± 1.2	7.2 ± 1.2
VET12-double [b]	0.39	3.4 ± 0.5	2.4 ± 0.5
VET18-tri [c]	0.39	3.3 ± 0.4	1.5 ± 0.2
VET24-quad [d]	0.39	3.4 ± 0.2	0.9 ± 0.1
TON6 [e]	0.52	3.4 ± 0.2	1.9 ± 0.2
VET6-tri [f]	0.13	11.3 ± 1.7	9.6 ± 1.2

[a] *6 water molecules in a simulation cell of length 7 unit cells; VET-type zeolite*
[b] *12 water molecules in a simulation cell of length 14 unit cells; VET-type zeolite*
[c] *18 water molecules in a simulation cell of length 21 unit cells; VET-type zeolite*
[d] *24 water molecules in a simulation cell of length 28 unit cells; VET-type zeolite*
[e] *6 water molecules in a simulation cell of length 7 unit cells; TON-type zeolite*
[f] *6 water molecules in a simulation cell of length 21 unit cells; VET-type zeolite*

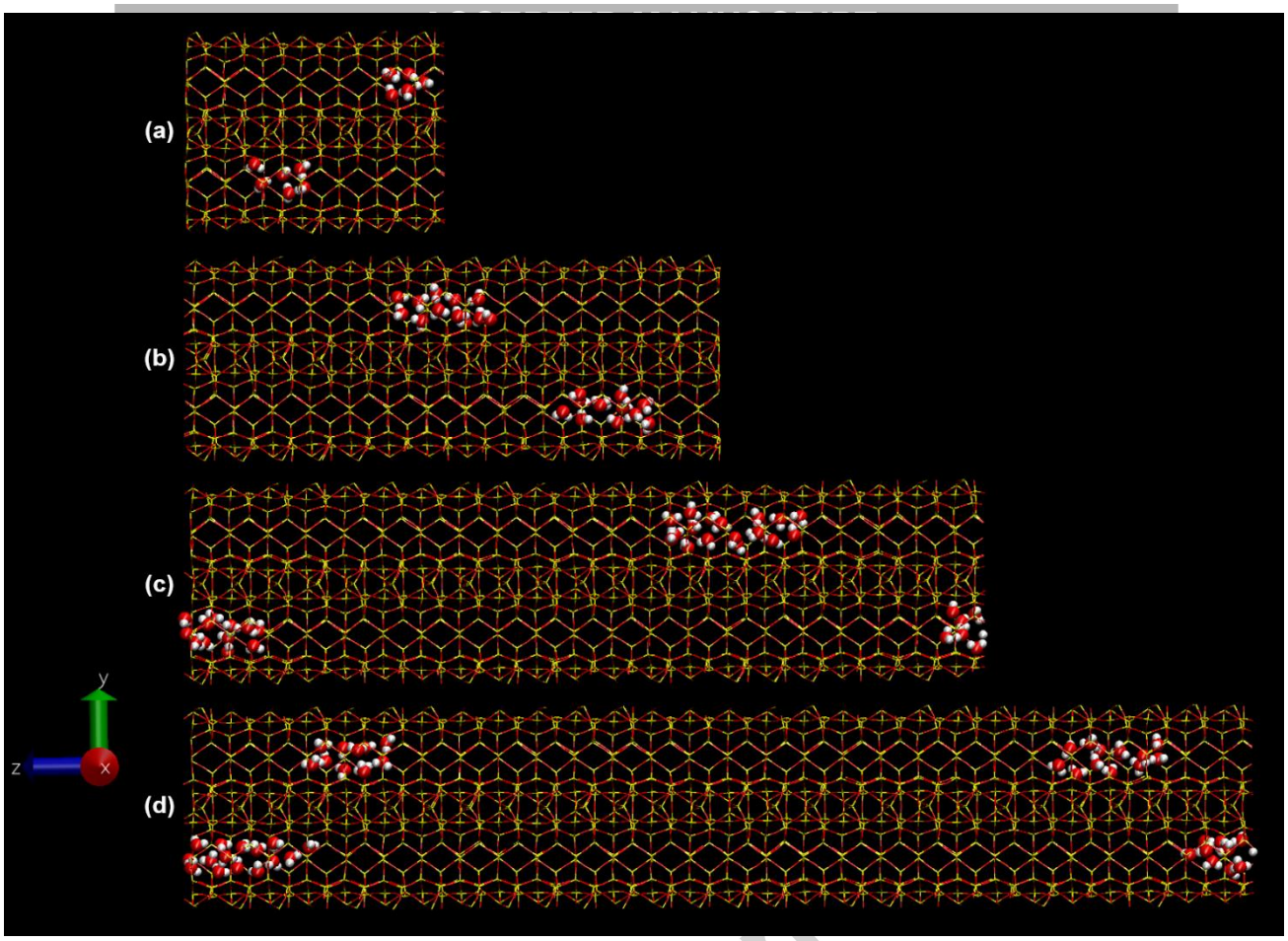

Fig. 8. Snapshots of (a) VET6, (b) VET12-double, (c) VET18-tri, and (d) VET24-quad (water represented by ball-and-sticks and zeolites by wires, oxygen coloured in red, hydrogen in white, silicon in yellow). Only water molecules in the front pores are shown for better visualisation.

As can be seen in Table 2, VET12-double, VET18-tri, and VET24-quad produce similar z-components of the self-diffusion coefficients ($3.3 – 3.4 \times 10^{-9}$ m^2 s^{-1}) but they are significantly lower than the self-diffusion coefficient in VET6. All diffusivities were determined from MSDs computed using the equations (3) and (4) in which MSDs of the confined water show linear diffusive regimes for all the extended zeolites. We also observe that the value of the z-component of the collective diffusion coefficient vary, seeming to converge to a value of about 0.9×10^{-9} m^2 s^{-1} when the VET24-quad system is considered. Experimentally, there exists an ideal droplet size and distribution. If this includes droplets with a larger number of water molecules than that existing in the periodic

cell, then that droplet cannot form. As the length of the pore, and hence the number of molecules in the periodic cell, increases (while keeping the density constant) the droplet size and its distribution will converge to the thermodynamic value.

As the number of the water molecules increases in the periodic system, the collective diffusivities will be lower as displayed in Table 2. Increasing the number of molecules allows formation of large clusters which diffuse less freely.

The results shown in $g_{pore}(r)$ in Fig. 9(a) clearly demonstrate differences in the water structure between VET6 and the extended zeolites. In VET6, $g_{pore}(r)$ drops below 1 at about 6 Å, suggesting that water clusters of 6 molecules exist and are quite stable. Comparing with VET12-double, VET18-tri, and VET24-quad we see several differences although the water densities are the same. Firstly, the first peak is higher. This is consistent with the formation of longer water clusters: the first peak represents the average number of water molecules directly bonded to the molecule of interest, or its coordination number. In a water cluster in a pore, the water molecules at the ends of the cluster will have lower coordination numbers than those in the centre of the cluster, and therefore the longer the cluster, the higher the average coordination number will be. This will also be evident in the height of the second peak. Comparison of the heights of the first peak with different simulation cell lengths indicates that the average cluster size is growing considerably as the number of water molecules increases from 6 to 12 (with corresponding increases in the length of the cell), and there is a further increase in VET18-tri with little change going to VET24-quad. The length of these clusters grows and from the images in Fig. 8, clusters of over 26 Å form in VET24, however several clusters can co-exist and clusters of 6 molecules are still common. The formation of long clusters is reflected in the fact that $g_{pore}(r)$ is still well above 1 in the region 7 - 8.5 Å in all cases considered in 9(a) except the VET6 system. These results indicate that in considering the relatively low water loadings where clusters tend to form, it is important to examine the system size effect before comparison of the results with experiment. Although the z-component of the self-diffusion coefficient in VET6 is

well above the self-diffusion coefficient of bulk water, a more reliable value is obtained using the longer simulations cells. It is interesting to observe that this value is also above that of bulk water and VET32, indicating that the clustering is resulting in enhanced self-diffusion. Comparison of the collective diffusion coefficient in VET24-quad with that in VET32 suggests that collective diffusion coefficient is only slightly lower at the higher loading, and that order of magnitude enhancement observed with VET6 was misleading.

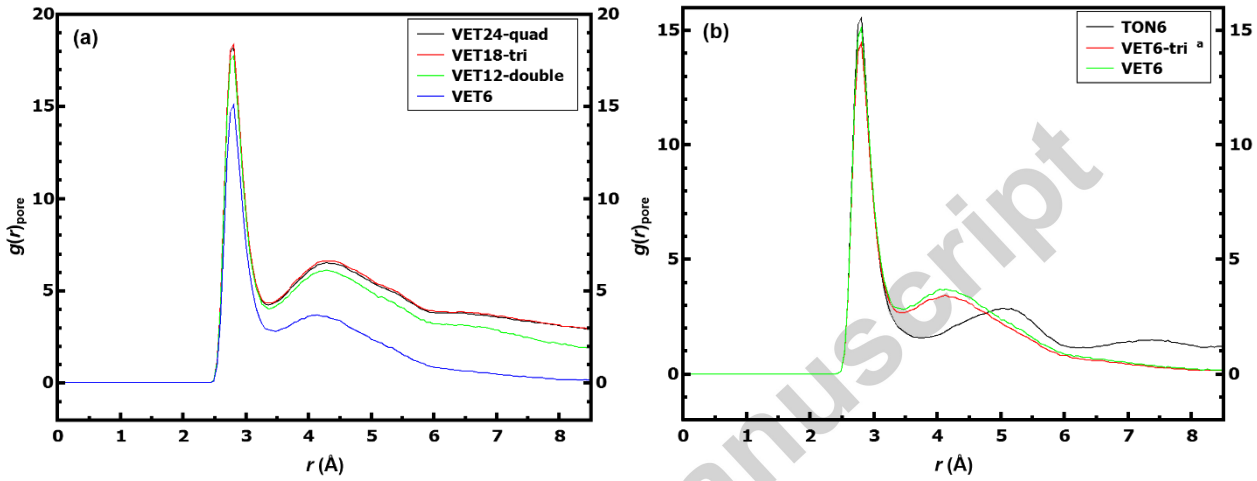

Fig. 9. The pore radial distribution function, $g_{pore}(r)$ for the O-O atoms of the water for (a) various loadings, and (b) different simulation cell lengths in different types of zeolites.

Considering VET24-quad, we can conclude that at lower loadings the self-diffusion coefficient (D_s = $D_{sz}/3$ = 1.1 × 10^{-9} m^2 s^{-1}) is about 5 times higher than that found in commercially used polyamide membranes when hydrated ca. 0.2 × 10^{-9} m^2 s^{-1} [59-61]. According to previous work on polyamide membranes, the hydrated membrane contains 23 wt% of water in the pores, meaning that the water density in the commercial membrane is 0.32 g/cm^3 which is similar to that of the lower loadings case (0.39 g/cm^3) in this study. We can also compare these results to those from different zeolite membrane candidates that have been previously determined: the self-diffusivities have been reported as 1.0 – 4.0 × 10^{-9} m^2 s^{-1} [23, 64-66] when 0.47 g/cm^3 of water is loaded in MFI zeolites, while

hydrated LTA zeolites have values of ~0.5×10^{-9} m^2 s^{-1} [11, 67]. Those values are comparable to and about 2 times lower than VET24-quad (1.1×10^{-9} m^2 s^{-1}), respectively. Given that MFI and LTA zeolites possess fully-connected 3-D pores, well-defined 1-D channels of VET will produce much higher water transport in one-direction than the 3-D pores. This high diffusivity can be associated with the hydrophobic nature of the pore which enhances the formation of nanodroplets. Even for the higher loadings, i.e. 32 water molecules per pore, diffusivities are approximately four times higher than the polyamide membranes, and the self-diffusion coefficient in the z-direction nearly corresponds to the self-diffusion coefficient for bulk water. At high loadings water-water interactions becomes dominant for the diffusive behaviour as opposed to water-zeolite interactions.

In VET6 and TON6, 6 water molecules were placed in simulation cells consisting of 7 unit cells, however due to the different pore sizes their number densities were different (0.39 g/cm^3 for VET6 and 0.52 g/cm^3 for TON6). Fig. 9(b) compares $g_{pore}(r)$ for these systems and the results indicate the water molecules do not form stable 6 membered clusters in TON6. The shifted second peak suggests the formation of chains of molecules, however the linearity of the MSD versus time indicates molecules can pass one another. Comparison of the snapshots in Fig. 10 and 6 verify this result and also indicate that the chains vary in length and are less stable. TON6 has a lower self-diffusion coefficient that VET6, and the self and collective diffusion coefficients differ, however it should be noted that the results are similar to those obtained for VET24-quad, and the collective diffusion coefficient is somewhat higher.

We also consider the effect of density on the results by comparing the results of 6 water molecules in a pore consisting of 21 unit cells in the z-direction (VET6-tri) with VET6. The VET6-tri (6 water molecules/triple-longer pore) results a slightly higher self and collective diffusivity than VET6, although the statistical significance of the difference is marginal. Fig. 9(b) compares $g_{pore}(r)$ for these systems and the results are very similar, indicating that the structures in the two cases are very similar. Presumably as the density of the water decreases, a phase change will occur and the clusters

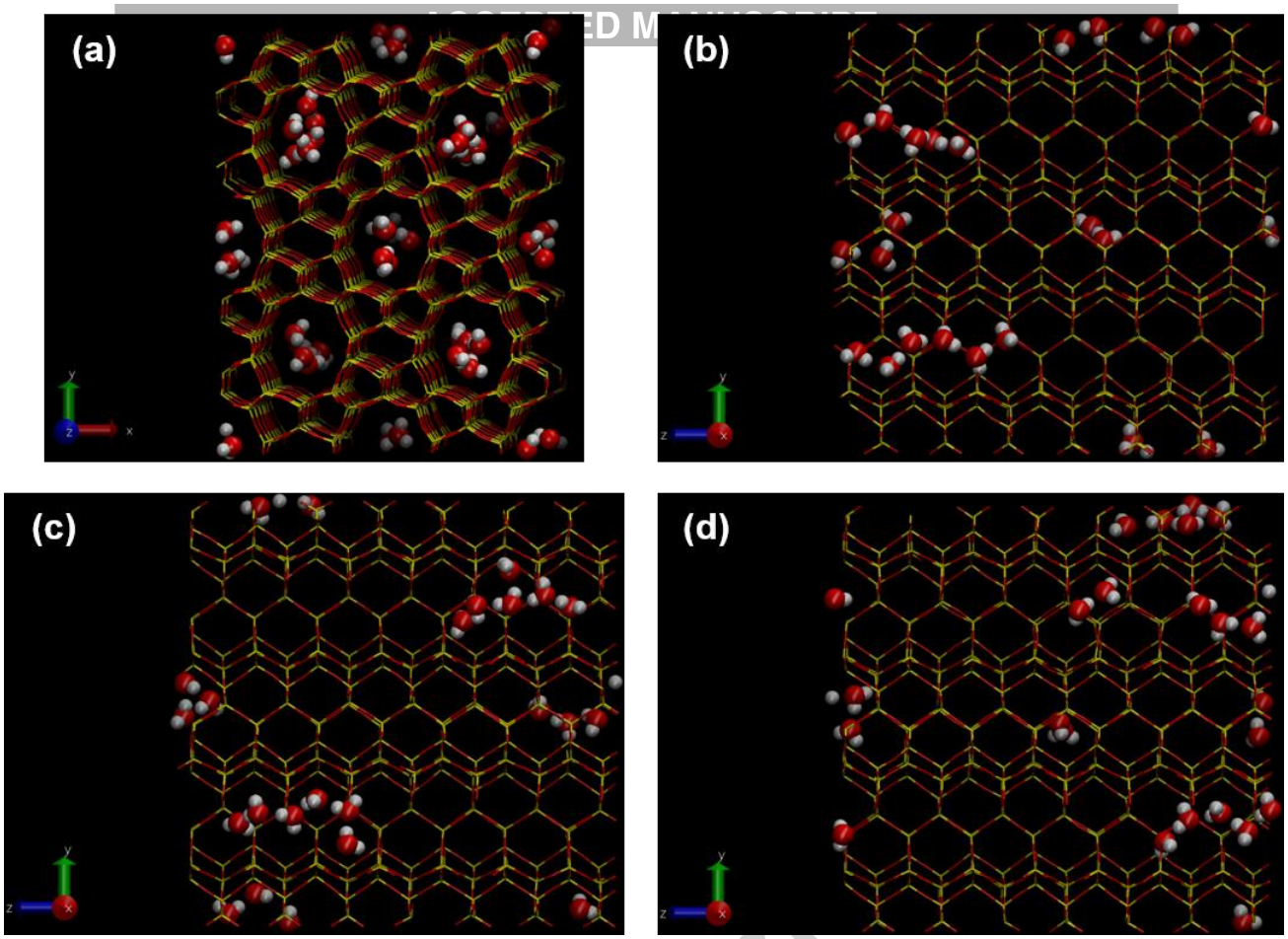

Fig. 10. Snapshots of TON6 simulations (water represented by ball-and-sticks and zeolites by wires, oxygen coloured in red, hydrogen in white, silicon in yellow): (a) view along the z-axis and (b)-(d) views along the x-axis initially, at 1000 ps, and at 2000 ps, respectively. Only water molecules in four of the pores are shown in (b)-(d), for better visualisation.

will dissociate, however even at this low density of 0.13 g/cm^3, this has not occurred. Effect of density difference and same density with different pore geometries on transport and structure of water confined in zeolites will be further studied in future work.

4. Conclusions

In this study, transport and structural properties of water inside zeolites were explored using MD simulations, with the aim of assessing a class of candidate zeolites as membrane materials. Force fields previously validated against experimental data were employed. Different thermostatting strategies were investigated. The thermostatting mechanism had little effect on the diffusion coefficients for water confined in a VET zeolite and even produced consistent results with those obtained from NVE and NPT simulations.

Long, narrow pores with the same loading and/or the same density were also examined. Considering low loadings of water, when the simulation cell size was increased while keeping the same density as VET6, self-diffusivities in the z-direction were observed to converge to ca. 3.4×10^{-9} m^2 s^{-1}. It should be noted that at low loadings, it is important to ensure that the number of unit cells along the pore is sufficient that convergence to thermodynamic behaviour is obtained or otherwise non-physical results are obtained due to the upper bound on the number of water molecules in the water cluster. For example the results obtained for VET6 (6 water molecules per pore) does not give an accurate prediction for the self-diffusion coefficient of a system with a loading of 0.39 g/cm^3 because it prevents the formation of clusters larger than 6 molecules.

TON6 has a comparable self-diffusivity to that of VET24-quad, but a higher collective diffusivity. This is because the water molecules did not form a stable cluster, resulting collective diffusivity being significantly lower than the self-diffusivity.

High diffusion rates for both low and high water loading were measured compared with polyamide membranes. The self-diffusivities for VET24-quad, VET32, and TON6 were all higher than for the polyamide membrane (ca. 0.2×10^{-9} m^2 s^{-1}) that are currently used for water desalination, suggesting that these materials may be useful. In particular, the fully-loaded VET32 had a comparable self-diffusion rate with bulk water (2.3×10^{-9} m^2 s^{-1}) even though the water density of VET32 was twofold higher (2.1 g/cm^3).

This study on the diffusional and structural properties of confined water in zeolites has analysed a number of important issues that need to be considered in evaluation of diffusion coefficients for fluids in pores using computational methods. It suggests that the one dimensional cylindrical pores can result in higher diffusivities, guiding the selection of future membranes for practical applications.

Acknowledgements

We would like to thank the Australian Research Council for support of this project through the LIEF program. This research was undertaken with the assistance of resources provided at the NCI National Facility systems at the Australian National University through the National Computational Merit Allocation Scheme supported by the Australian Government, support from the Queensland Cyber Infrastructure Foundation (QCIF) and the University of Queensland Research Computing Centre. We are also grateful to the University of Queensland and National Centre of Excellence in Desalination Australia for the UQI and top-up scholarships supporting a PhD program of the first author in this study. Lastly, we thank Dr. James Reid and Dr. Guozhao Ji from CTCMS and School of Chemical Engineering at UQ, respectively for their helpful discussion.

References

[1] S.M. Auerbach, K.A. Carrado, P.K. Dutta, Handbook of Zeolite Science and Technology, CRC Press, New York, 2003.

[2] M. Granda-Valdés, A.I. Pérez-Cordoves, M.E. Díaz-García, Zeolites and zeolite-based materials in analytical chemistry, Trends Anal. Chem. 25 (2006) 24-30.

[3] C. Baerlocher, L.B. McCusker, Database of Zeolite Structures, IZA-SC, 2014, URL: <http://www.iza-structure.org/databases/>.

[4] E.L. First, C.E. Gounaris, J. Wei, C.A. Floudas, Computational characterization of zeolite porous networks: an automated approach, Phys. Chem. Chem. Phys. 13 (2011) 17339-17358.

[5] J. Gascon, F. Kapteijn, B. Zornoza, V. Sebastian, C. Casado, J. Coronas, Practical Approach to Zeolitic Membranes and Coatings: State of the Art, Opportunities, Barriers, and Future Perspectives, Chem. Mater. 24 (2012) 2829-2844.

[6] M. Drobek, C. Yacou, J. Motuzas, A. Julbe, L. Ding, J.C. Diniz da Costa, Long term pervaporation desalination of tubular MFI zeolite membranes, J. Membr. Sci. 415–416 (2012) 816-823.

[7] K.P. Lee, T.C. Arnot, D. Mattia, A review of reverse osmosis membrane materials for desalination-Development to date and future potential, J. Membr. Sci. 370 (2011) 1-22.

[8] B. Zhu, C.M. Doherty, X.R. Hu, A.J. Hill, L.D. Zou, Y.S. Lin, M. Duke, Designing hierarchical porous features of ZSM-5 zeolites via Si/Al ratio and their dynamic behavior in seawater ion complexes, Microporous Mesoporous Mater. 173 (2013) 78-85.

[9] M.C. Duke, J. O'Brien-Abraham, N. Milne, B. Zhu, J.Y.S. Lin, J.C.D. da Costa, Seawater desalination performance of MFI type membranes made by secondary growth, Sep. Purif. Technol. 68 (2009) 343-350.

[10] D. Li, H.T. Wang, Recent developments in reverse osmosis desalination membranes, J. Mater. Chem. 20 (2010) 4551-4566.

[11] J. Lin, S. Murad, A computer simulation study of the separation of aqueous solutions using thin zeolite membranes, Mol. Phys. 99 (2001) 1175-1181.

[12] Z.E. Hughes, L.A. Carrington, P. Raiteri, J.D. Gale, A Computational Investigation into the Suitability of Purely Siliceous Zeolites as Reverse Osmosis Membranes, J. Phys. Chem. C 115 (2011) 4063-4075.

[13] Y. Liu, X. Chen, High permeability and salt rejection reverse osmosis by a zeolite nano-membrane, Phys. Chem. Chem. Phys. 15 (2013) 6817-6824.

[14] L. Wang, R.S. Dumont, J.M. Dickson, Nonequilibrium molecular dynamics simulation of pressure-driven water transport through modified CNT membranes, J. Chem. Phys. 138 (2013) 124701.

[15] D. Cohen-Tanugi, J.C. Grossman, Water permeability of nanoporous graphene at realistic pressures for reverse osmosis desalination, J. Chem. Phys. 141 (2014) 074704.

[16] J.K. Holt, H.G. Park, Y.M. Wang, M. Stadermann, A.B. Artyukhin, C.P. Grigoropoulos, A. Noy, O. Bakajin, Fast mass transport through sub-2-nanometer carbon nanotubes, Science 312 (2006) 1034-1037.

[17] A. Alexiadis, S. Kassinos, Molecular Simulation of Water in Carbon Nanotubes, Chem. Rev. 108 (2008) 5014-5034.

[18] D. Cohen-Tanugi, J.C. Grossman, Water Desalination across Nanoporous Graphene, Nano Lett. 12 (2012) 3602-3608.

[19] T. Ohba, H. Kanoh, K. Kaneko, Water cluster growth in hydrophobic solid nanospaces, Chem. 11 (2005) 4890-4894.

[20] P. Demontis, J. Gulín-González, H. Jobic, M. Masia, R. Sale, G.B. Suffritti, Dynamical Properties of Confined Water Nanoclusters: Simulation Study of Hydrated Zeolite NaA: Structural and Vibrational Properties, ACS Nano 2 (2008) 1603-1614.

[21] T. Iiyama, R. Aragaki, T. Urushibara, S. Ozeki, Direct Determination of the Intermolecular Structure of the Adsorbed Phase Using *in situ* X-Ray Diffraction and Reverse Monte Carlo Methods, Adsorpt. Sci. Technol. 24 (2006) 815-821.

[22] T. Ohba, K. Kaneko, Initial filling mechanism of predominant water adsorption on hydrophobic slit-shaped carbon nanopores, J. Phys.: Conf. Ser. 177 (2009) 012001.

[23] C. Bussai, S. Vasenkov, H. Liu, W. Böhlmann, S. Fritzsche, S. Hannongbua, R. Haberlandt, J. Kärger, On the diffusion of water in silicalite-1: MD simulations using ab initio fitted potential and PFG NMR measurements, Appl. Catal. A: Gen. 232 (2002) 59-66.

[24] Q. Zhang, K.-Y. Chan, N. Quirke, Molecular dynamics simulation of water confined in a nanopore of amorphous silica, Mol. Simul. 35 (2009) 1215-1223.

[25] M.U. Arı, M.G. Ahunbay, M. Yurtsever, A. Erdem-Şenatalar, Molecular Dynamics Simulation of Water Diffusion in MFI-Type Zeolites, J. Phys. Chem. B 113 (2009) 8073-8079.

[26] D.J. Evans, G. Morriss, Statistical Mechanics of Nonequilibrium Liquids, 2nd ed., Cambridge University Press, London, 2008.

[27] P. Hünenberger, Thermostat Algorithms for Molecular Dynamics Simulations, in: C. Holm, K. Kremer (Eds.) Advanced Computer Simulation, Springer Berlin Heidelberg, 2005, pp. 105-149.

[28] J.E. Basconi, M.R. Shirts, Effects of Temperature Control Algorithms on Transport Properties and Kinetics in Molecular Dynamics Simulations, J. Chem. Theory Comput. 9 (2013) 2887-2899.

[29] J.N. Bright, D.J. Evans, D.J. Searles, New observations regarding deterministic, time-reversible thermostats and Gauss's principle of least constraint, J. Chem. Phys. 122 (2005) 194106.

[30] T.V.S. Krishnan, J.S. Babu, S.P. Sathian, A molecular dynamics study on the effect of thermostat selection on the physical behavior of water molecules inside single walled carbon nanotubes, J. Mol. Liq. 188 (2013) 42-48.

[31] S. Bernardi, B.D. Todd, D.J. Searles, Thermostating highly confined fluids, J. Chem. Phys. 132 (2010) 244706.

[32] X. Yong, L.T. Zhang, Thermostats and thermostat strategies for molecular dynamics simulations of nanofluidics, J. Chem. Phys. 138 (2013) 084503.

[33] M. Thomas, B. Corry, Thermostat choice significantly influences water flow rates in molecular dynamics studies of carbon nanotubes, Microfluid. Nanofluid. 18 (2014) 41-47.

[34] Z. Chi, C. Luo, Y. Dai, Comment on "Electrical-Driven Transport of Endohedral Fullerene Encapsulating a Single Water Molecule", Phys. Rev. Lett. 113 (2014) 119601.

[35] S. Alberto, Water self-diffusion through narrow oxygenated carbon nanotubes, Nanotechnol. 18 (2007) 475704.

[36] K.E. Gubbins, Y.-C. Liu, J.D. Moore, J.C. Palmer, The role of molecular modeling in confined systems: impact and prospects, Phys. Chem. Chem. Phys. 13 (2011) 58-85.

[37] H. Jobic, J. Kärger, M. Bée, Simultaneous Measurement of Self- and Transport Diffusivities in Zeolites, Phys. Rev. Lett. 82 (1999) 4260-4263.

[38] W.F. Smith, J. Hashemi, Foundations of Materials Science and Engineering, 5th ed., McGraw-Hill, London, UK, 2009.

[39] F. Kapteijn, W.J.W. Bakker, G. Zheng, J. Poppe, J.A. Moulijn, Permeation and separation of light hydrocarbons through a silicalite-1 membrane: Application of the generalized Maxwell-Stefan equations, Chem. Eng. J. Biochem. Eng. J. 57 (1995) 145-153.

[40] D.C. Rapaport, The Art of Molecular Dynamics Simulation, 2nd ed., Cambridge University Press, Cambridge, UK, 2004.

[41] S.J. Plimpton, Fast Parallel Algorithms for Short-Range Molecular Dynamics, J. Comput. Phys. 117 (1995) 1-19.

[42] W. Shinoda, M. Shiga, M. Mikami, Rapid estimation of elastic constants by molecular dynamics simulation under constant stress, Phys. Rev. B 69 (2004) 134103.

[43] G.J. Martyna, D.J. Tobias, M.L. Klein, Constant pressure molecular dynamics algorithms, J. Chem. Phys. 101 (1994) 4177-4189.

[44] J.M. Thijssen, Computational Physics, 2nd ed., Cambridge University Press, Cambridge, UK, 2007.

[45] C.C. Freyhardt, R.F. Lobo, S. Khodabandeh, J.E. Lewis, M. Tsapatsis, M. Yoshikawa, M.A. Camblor, M. Pan, M.M. Helmkamp, S.I. Zones, M.E. Davis, VPI-8: A High-Silica Molecular Sieve with a Novel "Pinwheel" Building Unit and Its Implications for the Synthesis of Extra-Large Pore Molecular Sieves, J. Am. Chem. Soc. 118 (1996) 7299-7310.

[46] H.W. Horn, W.C. Swope, J.W. Pitera, J.D. Madura, T.J. Dick, G.L. Hura, T. Head-Gordon, Development of an improved four-site water model for biomolecular simulations: TIP4P-Ew, J. Chem. Phys. 120 (2004) 9665-9678.

[47] H.W. Horn, W.C. Swope, J.W. Pitera, Characterization of the TIP4P-Ew water model: vapor pressure and boiling point, J. Chem. Phys. 123 (2005) 194504.

[48] B. Smit, Phase diagrams of Lennard-Jones fluids, J. Chem. Phys. 96 (1992) 8639-8640.

[49] F. Jensen, Introduction to Computational Chemistry, 2nd ed., Wiley, UK, 2007.

[50] M.J. Sanders, M. Leslie, C.R.A. Catlow, Interatomic potentials for SiO2, J. Chem. Soc. Chem. Commun. (1984) 1271-1273.

[51] N.H. de Leeuw, S.C. Parker, Molecular-dynamics simulation of MgO surfaces in liquid water using a shell-model potential for water, Phys. Rev. B 58 (1998) 13901-13908.

[52] S.J. Plimpton, R. Pollock, M. Stevens, Particle-Mesh Ewald and rRESPA for Parallel Molecular Dynamics Simulations, in: Eighth SIAM Conference on Parallel Processing for Scientific Computing, Minneapolis, MN, 1997.

[53] J.-P. Ryckaert, G. Ciccotti, H.J.C. Berendsen, Numerical integration of the cartesian equations of motion of a system with constraints: molecular dynamics of n-alkanes, J. Comput. Phys. 23 (1977) 327-341.

[54] B.U. Felderhof, Fluctuation theory of single-file diffusion, J. Chem. Phys. 131 (2009) 064504.

[55] S. Alexander, P. Pincus, Diffusion of labeled particles on one-dimensional chains, Phys. Rev. B 18 (1978) 2011-2012.

[56] P.A. Fedders, Two-point correlation functions for a distinguishable particle hopping on a uniform one-dimensional chain, Phys. Rev. B 17 (1978) 40-46.

[57] K. Krynicki, C.D. Green, D.W. Sawyer, Pressure and temperature dependence of self-diffusion in water, Faraday Discuss. Chem. Soc. 66 (1978) 199-208.

[58] R. Mills, Self-diffusion in normal and heavy water in the range 1-45 deg, J. Phys. Chem. 77 (1973) 685-688.

[59] M. Ding, A. Szymczyk, F. Goujon, A. Soldera, A. Ghoufi, Structure and dynamics of water confined in a polyamide reverse-osmosis membrane: A molecular-simulation study, J. Membr. Sci. 458 (2014) 236-244.

[60] Z.E. Hughes, J.D. Gale, A computational investigation of the properties of a reverse osmosis membrane, J. Mater. Chem. 20 (2010) 7788-7799.

[61] Z.E. Hughes, J.D. Gale, Molecular dynamics simulations of the interactions of potential foulant molecules and a reverse osmosis membrane, J. Mater. Chem. 22 (2012) 175-184.

[62] S.K. Kannam, B.D. Todd, J.S. Hansen, P.J. Daivis, How fast does water flow in carbon nanotubes?, J. Chem. Phys. 138 (2013) 094701.

[63] T.X. Nguyen, S.K. Bhatia, Some Anomalies in the Self-Diffusion of Water in Disordered Carbons, J. Phys. Chem. C 116 (2012) 3667-3676.

[64] J.Z. Yang, Y. Chen, A.M. Zhu, Q.L. Liu, J.Y. Wu, Analyzing diffusion behaviors of methanol/water through MFI membranes by molecular simulation, J. Membr. Sci. 318 (2008) 327-333.

[65] K.L. Joshi, G. Psofogiannakis, A.C.T. van Duin, S. Raman, Reactive molecular simulations of protonation of water clusters and depletion of acidity in H-ZSM-5 zeolite, Phys. Chem. Chem. Phys. 16 (2014) 18433-18441.

[66] J. Caro, M. Bülow, J. Richter-Mendau, J. Kärger, M. Hunger, D. Freude, Nuclear Magnetic Resonance Self-diffusion Studies of Methanol-Water Mixtures in Pentasil-type Zeolites, J. Chem. Soc., Faraday Trans. 1, 83 (1987) 1843-1849.

[67] P. Demontis, J. Gulín-González, H. Jobic, G.B. Suffritti, Diffusion of Water in Zeolites Na A and NaCa A: A Molecular Dynamics Simulation Study, J. Phys. Chem. C 114 (2010) 18612-18621.

Graphical abtract

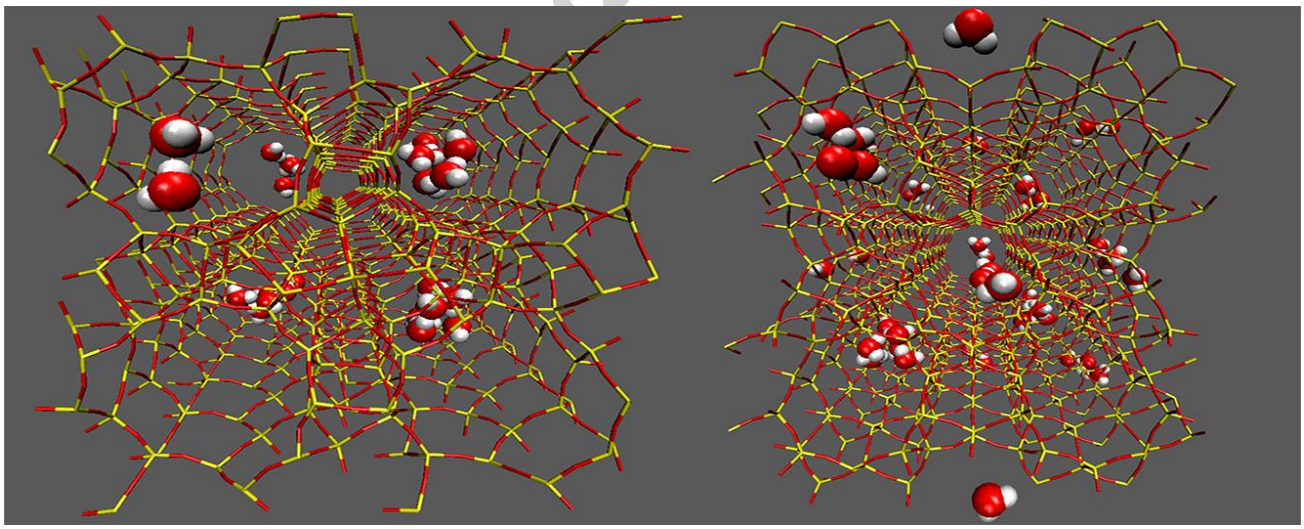

Highlights

- Transport and structural properties of water in zeolites were studied.
- The thermostatting mechanism had little effect on water diffusion rates.
- At low loadings, water molecules formed a cluster, which affected water transport.
- Zeolites showed higher water diffusivities than conventional membranes.
- Diffusion rates were influenced by water loading level, pore size and length.